Contents lists available at ScienceDirect

Arabian Journal of Chemistry

journal homepage: www.ksu.edu.sa

Well-synthesized carbon dots from flower of *Cassia fistula* and its hydrothermally grown heterojunction photocatalyst with zinc oxide (CDs@ZnO-H400) for photocatalytic degradation of ciprofloxacin and paracetamol

David Nugroho [a], Aphinya Thinthasit [a], Khemika Wannakan [b], Reggie Surya [c], Suwat Nanan [b,*], Rachadaporn Benchawattananon [a,*]

[a] *Department of Integrated Science, Faculty of Science, Khon Kaen University, Khon Kaen 40002, Thailand*
[b] *Materials Chemistry Research Center, Department of Chemistry and Center of Excellence for Innovation in Chemistry (PERCH-CIC), Faculty of Science, Khon Kaen University, Khon Kaen 40002, Thailand*
[c] *Food Technology Department, Faculty of Engineering, Bina Nusantara University, Jakarta 11480, Indonesia*

ARTICLE INFO

Keywords:
Carbon dots
Cassia fistula
Zinc oxide
Photocatalyst
Photodegradation

ABSTRACT

Pharmaceutical residues in aquatic environments have the potential to induce bacterial resistance, subsequently complicating disease treatment and posing a substantial hazard to public health. This study demonstrates the production of carbon dots from Cassia fistula flowers using a hydrothermal process. The obtained carbon dots were then mixed with zinc oxide to create CDs@ZnO-H400. This heterojunction photocatalyst exhibited notable enhancement in photocatalytic performance due to improved charge separation efficiency at the interface. The CDs@ZnO-H400 catalyst effectively removed two medications, ciprofloxacin and paracetamol. Ciprofloxacin showed maximum photocatalytic efficiency, with 99.8 % degradation, while paracetamol exhibited a degradation efficiency of 75.1 %. The stability of the synthesized photocatalyst was evaluated across four usage cycles using EDX-SEM, FTIR, and XRD techniques. The CDs@ZnO-H400 heterostructure photocatalyst maintained strong photoactivity even after the fourth cycle of usage.

1. Introduction

In recent years, there has been a growing apprehension regarding the existence of emerging toxins in the environment (Wang et al., 2022). This is mostly due to the limited understanding of the potential implications and long-term stability of these compounds in the environment (Dou et al., 2022; Zou et al., 2021). One of the most concerning developing pollutants pertains to pharmaceutical substances, which, as a result of their extensive human usage, are introduced into ecological systems. Drugs and their metabolites have been detected in several environmental sources such as wastewater, surface and deep water, soil, and air. The presence can be attributed mostly to the ingestion and elimination of drugs (or their metabolites), as well as the improper disposal of unused medications. The introduction of medicines into the aquatic environment can occur from various sources, including urban, hospital, industrial effluent, as well as wastewater derived from agricultural or livestock activities. Nevertheless, the primary concern regarding the existence of these pollutants, as well as their combinations, lies not only in their abundance but also in their enduring presence in the environment. This is due to the limited research conducted on sustained exposure to these pollutants (Trujillano et al., 2022; Almeida et al., 2020; Xu et al., 2022; Senasu et al., 2022; Patel et al., 2019). A growing body of ecotoxicology research indicates that medications are a potential hazard to aquatic creatures. The presence of medicines in several aquatic compartments and their bioaccumulation in numerous species serve as proof of this concern. Contaminants of Emerging Concerns (CEC), also referred to as emerging pollutants, encompass chemical substances that are found in water bodies but are not subject to environmental monitoring. These substances have the potential to adversely impact both ecological systems and human well-being. The substances that are currently gaining attention as emerging contaminants encompass medications, personal care items, endocrine disruptor

* Corresponding authors.
E-mail addresses: suwatna@kku.ac.th (S. Nanan), rachadaporn@kku.ac.th (R. Benchawattananon).

https://doi.org/10.1016/j.arabjc.2024.105931
Received 21 March 2024; Accepted 22 July 2024
Available online 23 July 2024

compounds, and pesticides (Azuma et al., 2019; Khan et al., 2020).

The drug known as paracetamol is widely used worldwide as an analgesic and antipyretic agent. The administration of paracetamol has been linked to the incidence of Stevens-Johnson syndrome and toxic epidermal necrolysis, two infrequent dermatological disorders that have the potential to result in mortality (Yang et al., 2008; Abdel-Wahab et al., 2017). Paracetamol has been observed in diverse aquatic habitats with quantities spanning from 3.3 ng/L to 16 μg/L (Fairbairn et al., 2016; Agunbiade and Moodley, 2014), while the values documented in saltwater exhibit a range of 3.2 ng/L to over 200 μg/L. The persistent and substantial intake and manufacturing of paracetamol, along with its apparent presence in saltwater, raise apprehensions regarding its potential effects on marine creatures, particularly those that rely on filtration (Benotti and Brownawell, 2007; Togola and Budzinski, 2008).

Ciprofloxacin, which was first introduced to the market in 1987, is categorized as a type of antibiotic belonging to the fluoroquinolone class. The utilization of these antibiotics is prevalent in the field of animal husbandry due to their broad spectrum of efficacy (Van Thuan et al., 2022; Queiróz et al., 2023; Behera et al., 2019; Costa et al., 2018). The utilization of these antibiotics is prevalent in the field of animal husbandry due to their broad spectrum of efficacy. Typically, the content of ciprofloxacin in water and wastewater was seen to range from around 150 μg L^{-1} to 21 mg L^{-1} (Li et al., 2017; Liu et al., 2019; Zhao et al., 2017). This antibiotic exhibit comparable toxicity to other antibiotics that have the potential to accumulate within the organism. Antibiotic compounds are introduced into the aquatic environment through several means, with medical antibiotic effluent being the most prevalent. The introduction of antibiotic residues into the soil and aquatic environment occurs via the ingestion of food by animals and humans (Ebert et al., 2011; Yang et al., 2017).

Carbon dots, also known as CDs, are two-dimensional quasi-spherical particles measuring less than 10 nm in size. They were initially identified in 2004 when purifying single-walled carbon nanotubes. CDs consist of carbon atoms that are hybridized with sp2/sp3 groups. CDs possess distinctive photophysical and chemical characteristics that set them apart from other carbon allotropes. These include a broad spectrum of light absorption, electron mediation, exceptional photostability, photosensitization, and low toxicity resulting from their nonmetallic composition. The aforementioned characteristics contribute to their extensive application in several fields, including photocatalysis, sensors, solar panels, medication delivery, and numerous other technological domains (Nugroho et al., 2022; Hou et al., 2017; Hu et al., 2021; Nugroho et al., 2024; Aghamali et al., 2018; Nugroho et al., 2022; Swapna and Sankararaman, 2019; Asadzadeh-Khaneghah et al., 2019). CDs possess inherent photocatalytic activity, which enables them to generate reactive oxygen species (ROS) upon exposure to light. These ROS, such as hydroxyl radicals ($^{\bullet}OH$) and superoxide radicals ($^{\bullet}O2^{-}$), are highly reactive species capable of oxidizing organic pollutants into smaller, less harmful molecules. One notable characteristic of carbon dots is their capacity to absorb visible light, which constitutes a substantial amount of sunlight. This attribute enables CDs to effectively capture solar energy, making them well-suited for photocatalytic purposes. CDs can undergo surface functionalization with different groups or metal nanoparticles in order to improve their photocatalytic efficiency. Functionalization can modify the surface characteristics of CDs, such as enhancing the quantity of active sites or enhancing charge separation, hence boosting their effectiveness in photodegradation reactions (Nugroho et al., 2024; Dervishi et al., 2019; Huang et al., 2019). The utilization of semiconductor photocatalysis has attracted considerable scholarly interest as a viable approach for the purification of water and air, as opposed to alternative conventional methods of pollution treatment (Yan et al., 2020; Zhang et al., 2021). Because of the characteristics of CDs, many researchers try to apply synthesis of carbon dots from various natural resources and apply them in photodegradation (Table 1). In instances when crystal development cannot be well regulated, the application of clean technology in the fabrication of photocatalyst nanostructures has resulted in the detection of sample aggregation. To effectively tackle the issue under consideration, a variety of capping agents were employed during the preliminary stage to precisely control the shape and photocatalytic properties of the catalysts (Folawewo and Bala, 2022; Chopra, 2022; Cheng et al., 2024; Xu et al., 2024; Lu et al., 2020; Zhou et al., 2023; Lu et al., 2022). The ZnO photocatalyst has garnered considerable interest due to its remarkable transport properties, cost-effectiveness in manufacture, and versatile shape. The actual implementation of ZnO is constrained by two main factors: inadequate ability to withstand sunshine and susceptibility to photocorrosion (Meky et al., 2024; Chehhat et al., 2023; Ramos et al., 2023). Previous studies have utilized photocatalysis techniques to degrade antibiotic contaminants and paracetamol, as indicated in Table 2.

This study aimed to synthesize and examine the photodegradation of ciprofloxacin and Paracetamol in water using a mixture of carbon dots derived from *Cassia fistula* and zinc oxide in various condition (CDs, CDs@ZnO and CDs@ZnO-H400). The synthesized materials were then analyzed and their photocatalytic activity performance was determined by treating them with ciprofloxacin and paracetamol in water. The study aimed to investigate and compare the impact of several factors, including the concentration of ciprofloxacin and paracetamol, the dose of CDs@ZnO-H400 catalyst powder, initial solution pH, addition of various scavengers, and reusability of the prepared CDs@ZnO-H400 photocatalyst.

2. Material and methods

2.1. Material

The flowers of Cassia fistula were taken from a flower garden located near Faculty of Science, building 01, Khon Kaen University in April 2023. All chemical reagents used in this research, including zinc oxide, are of analytical quality. Zinc Oxide was purchased from Sigma Aldrich. Paracetamol ($C_8H_9NO_2$) was purchased from commercial paracetamol with brand Tylenol (500 mg) and Ciprofloxacin ($C_{17}H_{18}FN_3O_3$) was purchased from commercial Ciprofloxacin with brand Cifloxin (500 mg) in the pharmacy store student food store Khon Kaen University, Thailand.

Table 1
Comparison carbon dots as a catalyst powder for photodegradation.

Catalyst name	CDs Source	Pollutant	%Photodegradation	Light Source	Ref.
mpg-C3N4/CQDs	Citric Acid	Paracetamol	85 %	Visible Light	(Wang et al., 2018)
CDs/ZnO-H400	Coconut water	Ofloxacin	99 %	Solar Light	(Nugroho et al., 2024)
CDs/ZnO-H400	Coconut water	RR141	99 %	Solar Light	(Nugroho et al., 2024)
ZnO/CD NCs	(NH4)2CO3	Ciprofloxacin	**98 %**	Solar Light	(Mukherjee et al., 2021)
CQDs/ZnO	$Zn(NO_3)_2{\cdot}6H_2O$	RhB	**99 %**	Visible Light	(Xu et al., 2023)
CQD-S2	citric acid, urea, polyethyleneimine.	rhodamine B (RhB)	99 %	Uv Light	(Ahlawat et al., 2023)
CDs@ZnO-H400	***Cassia fistula***	**Ciprofloxacin**	**99 %**	**Visible Light**	**This Work**
CDs@ZnO-H400	***Cassia fistula***	**Paracetamol**	**75 %**	**Visible Light**	**This Work**

Table 2
Comparison various carbon dots for degradation antibiotics

Catalyst Powder	Antibiotics Pollutants	% Photodegradation	Light Sourch	Ref.
ZnO-doped g-C3N4	Ciprofloxacin	94 %	**Visible Light**	(Van Thuan et al., 2022)
CeO2	Ciprofloxacin	89 %	**Uv Light**	(Queiróz et al., 2023)
ZnFe2O4@RGO	Ciprofloxacin	73 %	**Solar Light**	(Behera et al., 2019)
TiO_2 (Degussa P25)	Ciprofloxacin	22 %	**Visible Light**	(Sanchez Tobon et al., 2022)
CDs@ZnO-H400	**Ciprofloxacin**	**99 %**	**Visible Light**	**This Work**
TiEt400	Paracetamol	46 %	**Uv Lamp**	(Trujillano et al., 2022)
TiO_2	Paracetamol	89 %	**Uv Lamp**	(Yang et al., 2008)
TiO_2/Fe_2O_3	Paracetamol	94 %	**Uv Lamp**	(Abdel-Wahab et al., 2017)
TiO_2 (Degussa P25)	Paracetamol	83 %	**Uv Light**	(Jallouli et al., 2017)
La-doped ZnO	Paracetamol	85 %	**Visible Light**	(Thi and Lee, 2017)
CDs@ZnO-H400	**Ciprofloxacin**	**75 %**	**Visible Light**	**This Work**

2.2. Synthesis of Cassia fistula carbon dots (CDs)

Cassia fistula fresh flower has been washing several times using DI water, dried in the oven 75 °C for 48 h, after dry grind to become powder, and kept in the room temperature. For the future analysis.

3. Gram of Cassia fistula powder mixed with 40 ml DI water in the hydrothermal Teflon, after that put in the oven 180 °C, for 4 h (Nugroho et al., 2024). After synthesis, the carbon dots have been centrifuging 10000 rpm for 10 min, and filtered by using nylon membrane filter 0.22 µm, after that to become powder the carbon dots dry in the oven 75 °C for 48 h. (Nugroho et al., 2022; Nugroho et al., 2024)

3.1. Synthesis of CDs@ZnO by hydrothermal

A mixture of 1 g of CDs mixed with 10 mL of DI water and added 0.1-gram ZnO was prepared using a hydrothermal method. The mixture was heated in an oven at a temperature of 180 °C for 4 h. After the synthesis, the mixture was dried in the oven for 24 h to get a powdered and kept in the room temperature (Nugroho et al., 2024).

3.2. Synthesis of CDs@ZnOH-400 by calcination methods

To achieve the purification of CDs@ZnO, a quantity of 1 g of the CDs@ZnO powder was calcination for 4 h at a temperature of 400 °C. This was done using a closed system. (Nugroho et al., 2024).

3.3. Photodegradation of pollutants

Photocatalytic activity will be process by using mercury lamp (125 W) by measuring its ability to degrade the ciprofloxacin (CPF) and the paracetamol (PCT). The generated 50 mg of photocatalyst was mixed with a final volume (200 mL) of prepared pollutant solution with a concentration of 10 mg L^{-1}. To create an equilibrium condition of adsorption–desorption for the photocatalyst, the suspension was shaken for 60 min in a dark room condition. (5) mL sample was taken and centrifuged at 5000 rpm for 10 min, The purpose of this centrifugation process was to extract the supernatant (Senasu et al., 2022; Senasu et al., 2021).

The concentration assay was performed by quantifying the absorbance at wavelengths of 277 nm for CPF (Rajia et al., 2015) and 243 nm for paracetamol (Manu et al., 2011), respectively. In order to evaluate the %degradation, the equation for photodegradation efficiency was utilized, $(\%) = ((1 - C/C_0) \times 100\ \%)$. The equation presented above serves to quantify the extent of degradation by assessing the difference between the starting concentration (C_0) and the total amount of the contaminant in aqueous solution (C) after a predetermined period of irradiation. The degradation of the pollutant through photocatalysis can be described by a kinetic model, which can be mathematically represented by the first-order reaction rate equation, $\ln(C_0/C) = k_1 t$, where k_1 represents the rate constant associated with the first-order reaction. The primary focus of this work was to investigate the impact of different experimental factors, such as the initial pH of the solution, the loading of the photocatalyst, and the initial quantity of pollutants, on the observed photoactivity during the measurement of dye and antibiotic degradation. To examine the primary species accountable for the removal of the pollutant, this study introduced individual scavengers, namely potassium iodide (KI), benzoquinone (BQ), and isopropyl alcohol (IPA), at a concentration of 5 mM. The purpose of employing these scavengers was to selectively neutralize hydroxyl radicals, superoxide anion radicals, holes, and electrons, respectively (Nugroho et al., 2024; Senasu et al., 2022; Senasu et al., 2021).

3.4. Characterization

The instruments used for analysis include UV–visible spectrophotometers, X-ray photoelectron spectrometers (KRATOS AXIS SUPRA), Fourier Transform Infrared Spectrometers (FT-IR) (Bruker TENSOR 27), FIB-SEM (Helios NanoLab G3 CX), High-Resolution Transmission Electron Microscopes (HR-TEM) (Spectrometer: Transmission Electron Microscope; Electron gun: Schottky field emission type electron gun), Energy Dispersive X-ray Spectrometers (EDX) (Oxford Instruments X-Maxn), and ultraviolet–visible (UV–vis) diffused reflectance spectrometers (Shimazu UV–VISNIR-3101PC scanning spectrophotometer).

4. Results and discussions

4.1. Characterization of catalyst powder CDs@ZnO-H400

The Tauc-plot of the band gap energy of CDs, ZnO, CDs@ZnO, and CDs@ZnO-H400 photocatalysts is depicted in Fig. 1b. The energy bandgaps of CDs, ZnO, CDs@ZnO, and CDs@ZnO-H400 were determined to be 3.63, 3.19, 3.08, and 2.96 eV, respectively. The CDs@ZnO-H400 show the lowest bandgap energy after calcination process in the 400 °C, Calcination can lead to alterations in the composition of the material, such as the elimination of contaminants or the rearrangement of elements. The alterations can impact the band structure of the material, potentially resulting in a decrease in the bandgap energy (Lin et al., 2013; Cai et al., 2016). The enhanced photocatalytic effectiveness of CDs@ZnO-H400 photocatalyst can be attributed to its low bandgap energy. This can be achieved by utilizing the equation $E_{bg} = hc/\lambda$ (eV) to determine the bandgap energy (Wannakan et al., 2023). The diffused reflectance spectra (DRS) depicted in the Fig. 1a are employed for this purpose.

The X-ray diffraction patterns of CDs, CDs@ZnO, and CDs@ZnO-H400 (Fig. 1c) exhibited several peaks in the 2θ range, suggesting the

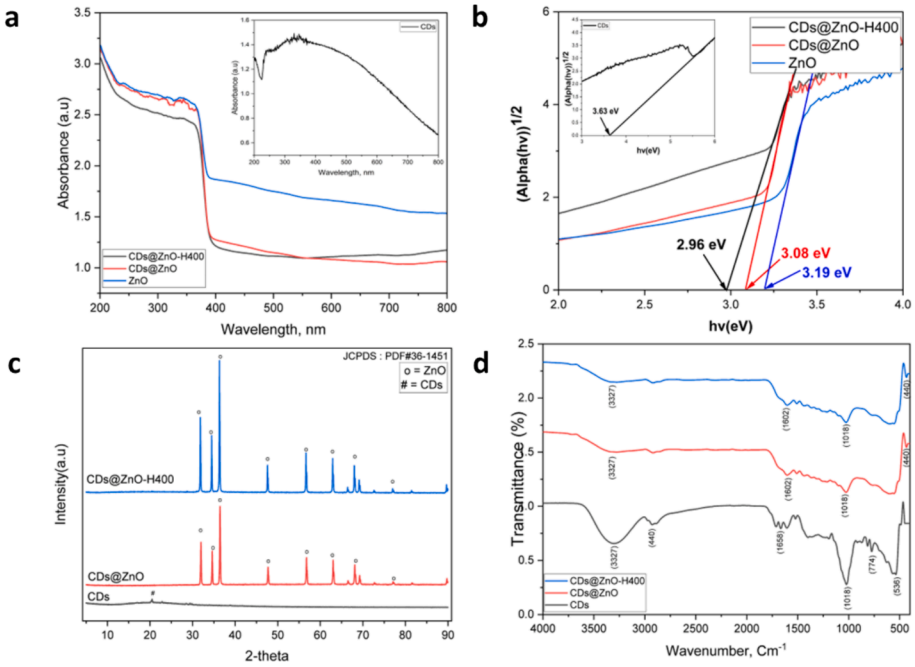

Fig. 1. Diffused reflectance spectra (DRS) (a), Tauc-plot for determination of band gap energy (b), XRD patterns (c), and FTIR spectra of the prepared photocatalysts (d).

presence of a significant crystal peak and diffraction peaks linked to the ZnO. at 2θ = 31.7° (1 0 0), 34.6° (0 0 2), 36.2° (1 0 1), 47.7° (1 0 2), 56.6° (1 1 0), 62.7° (1 0 3), and 67.8° (1 1 2), reflection planes, peaks of *Cassia fistula* carbon dots in the position 20.8° (0 0 2), Consequently, the hexagonal crystal structure of ZnO is verified (JCPDS: PDF#36–1451). The Crystallite size of each catalyst powder has been calculated and shows in the Table 3, the average crystal size of CDs, CDs@ZnO, and CDs@ZnO-H400 is 0.2, 38.9 and 41.69 nm, respectively. The XRD peak of ZnO indicates that it is the predominant crystal form and exhibits the highest level of photocatalytic activity compared to other crystal forms. This is attributed to the presence of a thin layer of one material on the surface of another material, which allows for interaction with the substrate material and consequently leads to a modification in the nearby crystal structure. Interface. Furthermore, it was noted that some diffraction peaks exhibited a more significant displacement as a result of the doping process (Nugroho et al., 2024; Ramos et al., 2023; Senasu et al., 2021; Song and de Villiers, 2005).

Table 3
Calculation of 6 Crystallite size catalyst powder.

Name of catalyst	Peak Position 2 theta	FWHM	Crystal size D (nm)	average (nm)
CDs@ZnO-H400	100	0.17	47.9	41.69
	002	0.17	48.6	
	101	0.17	47.9	
	102	0.22	38.7	
	110	0.25	36.4	
	103	0.26	35.6	
	112	0.26	36.7	
CDs@ZnO	100	0.19	43.3	38.9
	002	0.20	41.7	
	101	0.18	46.5	
	102	0.22	39.0	
	110	0.26	34.7	
	103	0.25	37.3	
	112	0.32	30.0	
CDs	002	31.8	0.2	0.2

The functional groups of CDs, CDs@ZnO, and CDs@ZnO-H400 were investigated using FTIR analysis, as illustrated in Fig. 1d. The experimental findings demonstrate the existence of the O–H stretching band at about 3327 cm^{-1}, the alkane bond of the C–H bond at 2940 cm^{-1}, a notable C═O bond at 1658 cm^{-1}, C-O stretching at 1018, 774, and 536 cm^{-1}, and the Zn-O bond at 440 cm^{-1} individually (Nugroho et al., 2024; Nugroho et al., 2022; Khan et al., 2015). The surface composition and chemical environment of CDs@ZnO-H400 composites were investigated using XPS measurements. The survey XPS spectra of CDs@ZnO-H400 revealed the presence of Zn2p, C1s, and O1s, as depicted in Fig. 2a. The peaks seen at the Zn2p level (Fig. 2b) were attributed to Zn2p3/2 and Zn2p1/2, with binding energies of 1022.5 and 1046.1 eV, respectively (Xu et al., 2013). Fig. 2c displays the high-resolution of C1s, revealing the prominent peak at 289.1 eV, which corresponds to the O-C═O bond. Additionally, another peak at 285.2 eV indicates the presence of C–C bonding (Yan et al., 2004; Bao et al., 2010). The high-resolution spectrum of O1s is depicted in Fig. 2d. The C–OH bond is responsible for the prominent peak observed at 532.9 eV. The second peak, seen at 532.1 and 530.2 eV, corresponds to C-O bonding and OL, respectively (Chen et al., 2010; Raja et al., 2016).

The morphological and characteristic of CDs@ZnO-H400 powder also has been studied under EDX-SEM and TEM. As shown in the Fig. 3a, the character of CDs is unstructured and easy to melting in the room temperature, Fig. 3b show the characteristic of ZnO a nd it's show that ZnO has a spherical and short-rod shape, and the Fig. 3c shows the CDs and ZnO are seen bonding to each other which can be observed from the large zinc oxide crystals with carbon dots which appear as small dots at the edge of the ZnO crystals. Fig. 3d depicts the properties of carbon dots (CDs) derived from Cassia fistula, with an average particle size of 6 nm. Fig. 3e illustrates the properties of CDs@ZnO-H400 under TEM, revealing the bonding between carbon dots and ZnO. The elemental of CDs@ZnO-H400 has been analyzed by using EDX. As shown in Fig. 3f, the atomic% of elemental C, O, and Zn, is 39.08, 29.93 and 29.61 %, respectively. In addition, the mapping of elemental under EDX was also displayed in the Fig. 3g–i.

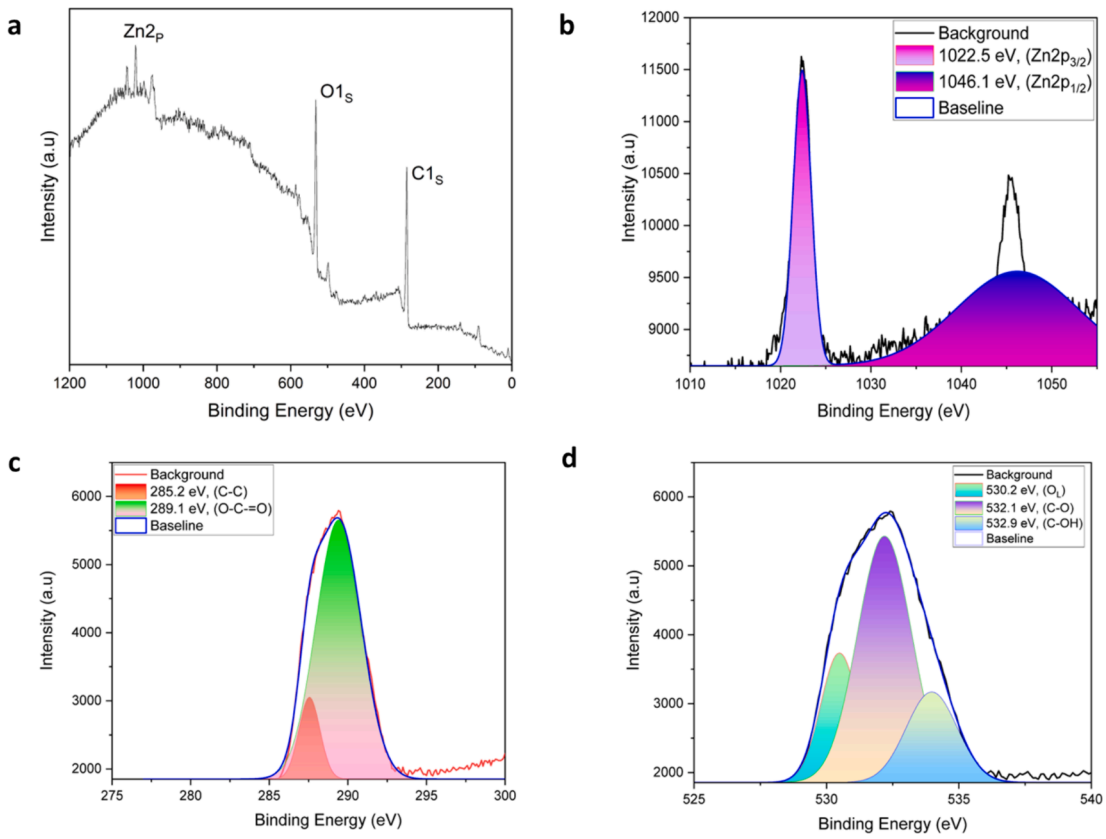

Fig. 2. XPS spectra of CDs@ZnO-H400: survey scan (a), Zn2p (b) O1s (c), and C1s (d).

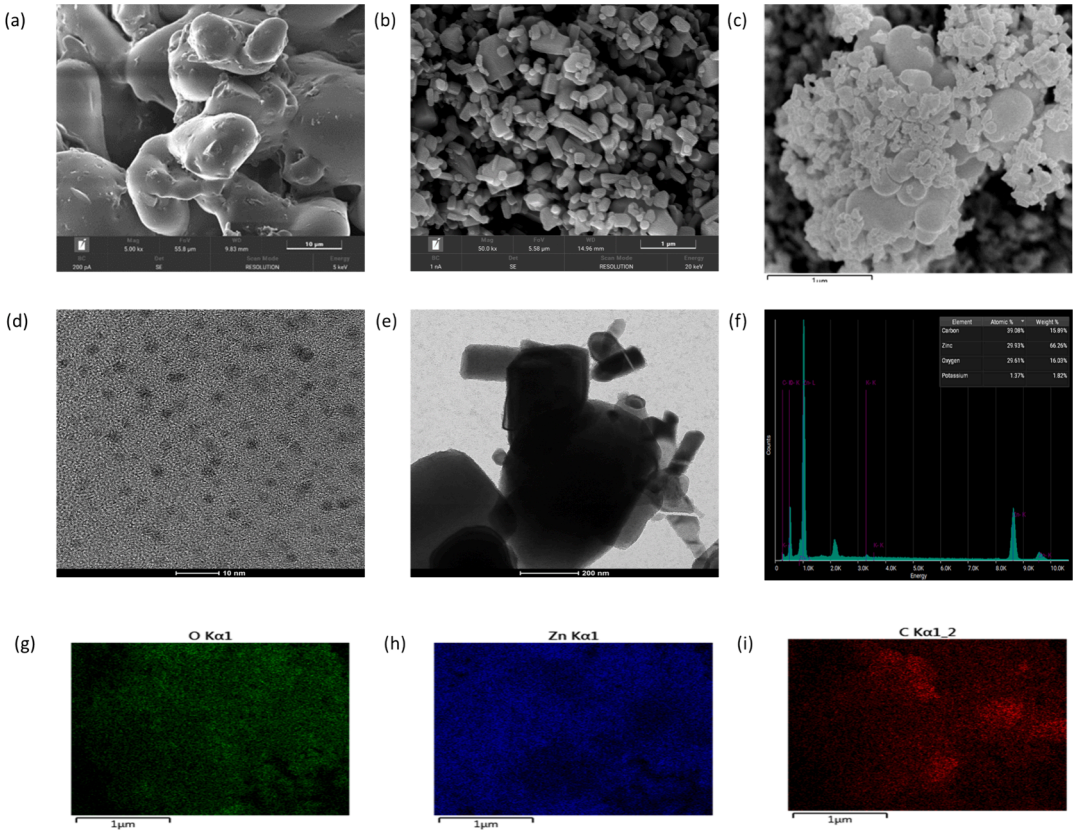

Fig. 3. SEM of CDs (a), Zinc Oxide (b) and CDs@ZnO-H400 (c) TEM of CDs (d) CDs@ZnO-H400 (e), EDX spectra of CDs@ZnO-H400 (f) mapping spectra of CDs@ZnO-H400 (g–i).

4.2. Photodegradation of various pollutants

This research examines the impact of ciprofloxacin (CPF) and paracetamol (PCT) as pollutants and investigates the catalytic degradation activity of several catalyst powders, CDs, CDs@ZnO, and CDs@ZnO-H400. The photodegradation process is simulated using solar light activation under a UV lamp. The standard tests employed in this study have demonstrated the presence of pollutants in the absence of diverse catalyst powders. The decomposition of CPF by CDs, CDs@ZnO, and CDs@ZnO-H400 nanostructures was observed to be around 44.7 %, 86.3 %, and 99.8 %, with the rate constant (k) of 6.078 E-4, 0.005, and 0.061 min^{-1} respectively, as depicted in Fig. 4a–c. In Fig. 4a–c, it can be observed that the catalysts of CDs, CDs@ZnO, and CDs@ZnO-H400 nanostructures exhibit decomposition efficiencies of approximately

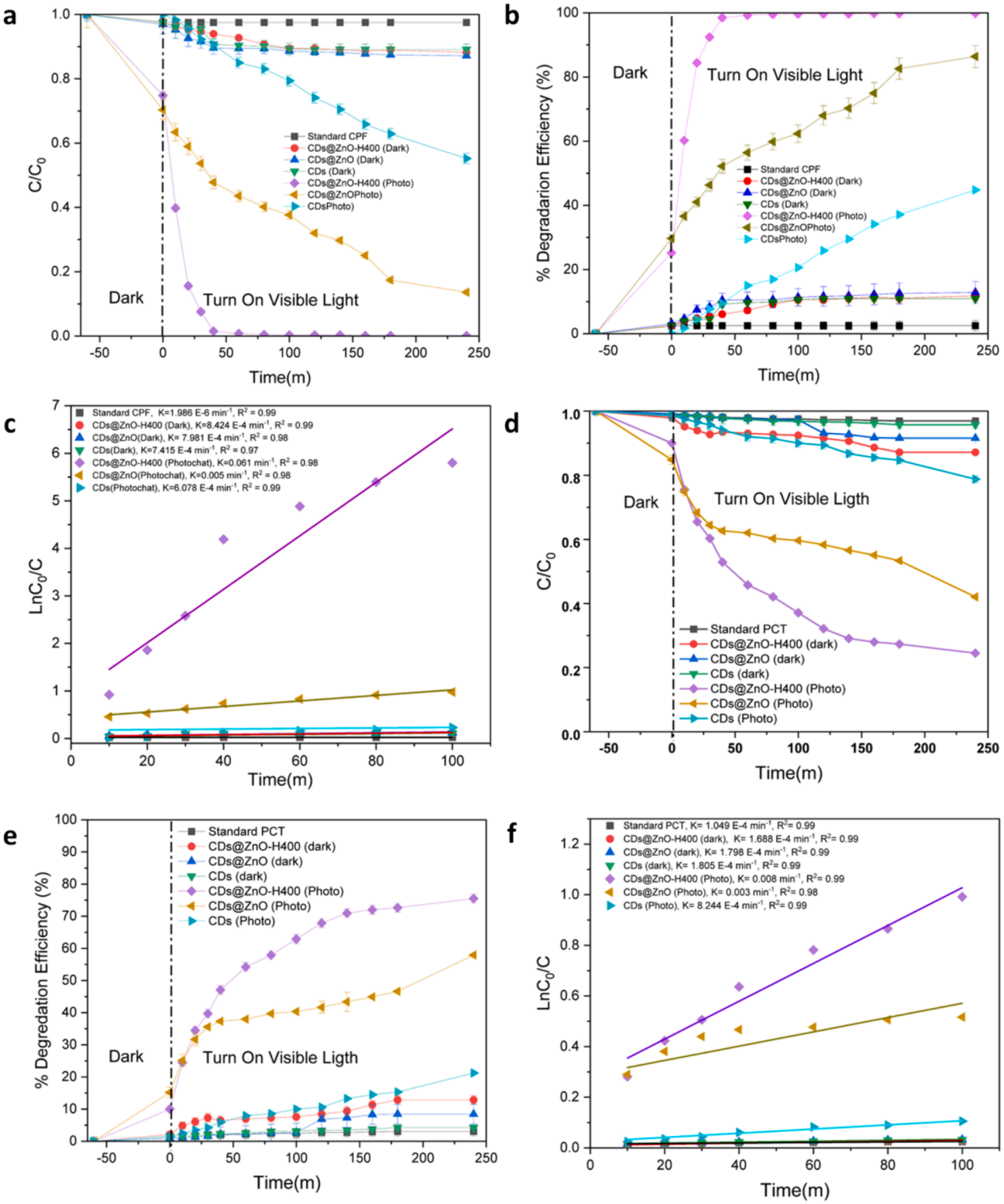

Fig. 4. Lowering of C/C_0 with time toward degradation of Ciprofloxacin (a), %degradation (b), determination of rate constant (c), lowering of C/C_0 with time toward degradation of Paracetamol (d), %degradation (e), and determination of rate constant (f). (n = 3).

21.2 %, 57.9 %, and 75.14 % for PCT, with the rate constant (k) 9.067 E-4, 0.002, and 0.007 min^{-1} respectively. The poor efficiencies observed in CDs can be attributed to their low optical efficiency and the presence of a significant number of electron-hole pairs (Khan et al., 2015; Nugroho et al., 2024; Kakarndee and Nanan, 2018). The CDs@ZnO nanocomposite demonstrated a notably greater photocatalytic degradation activity for both pollutants compared to individual CDs when subjected to identical circumstances. The application of calcination at a temperature of 400 °C has been seen to enhance the electron-hole separation efficiency of CDs@ZnO, resulting in a superior performance compared to other methods, the Calcination can stimulate or augment the photocatalytic activity, enhance the stability and longevity of materials, rendering them more resilient to severe photodegradation conditions, and eliminate impurities or pollutants found in the initial substance, which could otherwise hinder the photodegradation process or diminish the effectiveness of photocatalysts. Scheme 1–8 depicts a potential photocatalytic process that exhibits exceptional decomposition efficiency for CPF and PCT through the utilization of a CDs@ZnO-H400 catalyst nanocomposite. The heterogeneous connections formed in the CDs@ZnO-H400 catalyst nanocomposite are crucial for the migration

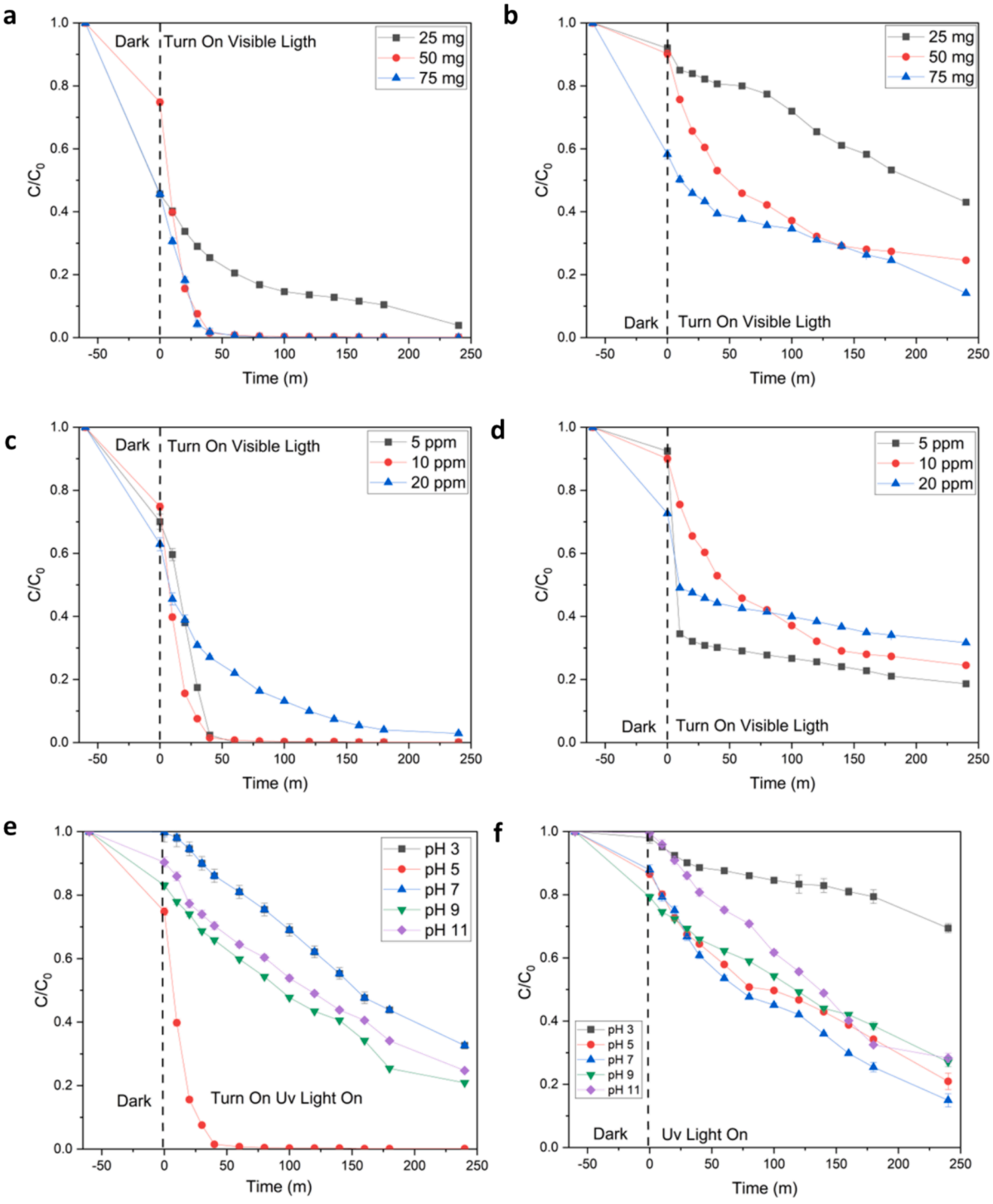

Fig. 5. Effect of catalyst loading on degradation of ciprofloxacin (a) and Paracetamol (b), effect of pollutant concentration on degradation of ciprofloxacin (c) and Paracetamol (d), effect of solution pH on degradation of ciprofloxacin (c) and Paracetamol (d). (n = 3).

and transmission of photo-excited charge carriers (Nugroho et al., 2024; Chankhanittha et al., 2021; Yu et al., 2021; Yu et al., 2024; Yu et al., 2021; Nie et al., 2022; Yang et al., 2023).

$$CDs + ZnO + hv \rightarrow CDs + ZnO + e^- + h^+ \quad (1)$$

$$h^+ + H_2O \rightarrow OH + H^- \quad (2)$$

$$h^+ + OH- \rightarrow OH \quad (3)$$

$$e^- + O_2 \rightarrow O_2 \quad (4)$$

$$O_2 + H + \rightarrow HO_2 \quad (5)$$

$$O_2 + \text{Pollutant} \rightarrow \text{Degradation Product} \quad (6)$$

$$e^- + \text{Pollutant} \rightarrow \text{Degradation Product} \quad (7)$$

$$OH + \text{Pollutant} \rightarrow \text{Degradation Product} \quad (8)$$

Experimental parameters' influence on photoactivity was conducted under many situations to determine the optimal conditions. These variables encompassed the influence of pH, catalyst content, and pollutant concentration (Fig. 5). The effect of catalyst loading has been study for degradation of CPF and PCT. The optimum condition for CPF is 50 mg (Fig. 5a) and that for PCT is 75 mg (Fig. 5b). The observed phenomenon can be attributed to the concurrent increase in the quantity of pollutants adsorbed onto the catalyst and the corresponding rise in the density of catalyst particles inside the photo-illuminated region (Chankhanittha et al., 2019). The various concentrations of pollutant have been studied in for CPF (Fig. 5c) and for PCT (Fig. 5d). The result shows that the concentration of pollutant influences on the resultant photoactivity. Under the condition of 20 ppm pollutant, the % degradation of CPF decreases to be 97,1% and PCT 68.3 %, respectively. Elevating the levels of pollutants leads to a decrease in photoactivity. When the concentration of pollutants is elevated, the pollutant molecules exhibit a substantial absorption of light, rather than the CDs@ZnO-H400 photocatalyst. Consequently, there is a reduction in the quantity of light that reaches the catalyst's surface, leading to a decline in the degrading efficiency (Senasu et al., 2021; Khan et al., 2015). The various concentration of pH has been tested for the influence study of photodegradation by using CDs@ZnO-H400 (pH range 3, 5, 7, 9 and 11) for CPF (Fig. 5e) and for PCT (Fig. 5f). The result shows that the degradation of CPF and PCT at pH of about 3 has significantly decreased to about 53.6 %. This is due to the fact that the CDs and ZnO has been dissolution in the acid condition. Thus, the optimum condition of degradation pollutant by using CDs@ZnO-H400 it's shown in the pH range 5 – 7. The increase in anionic pollutants can be attributed to the presence of catalyst powder (Kakarndee and Nanan, 2018). The CPF solution has a natural pH of approximately 6, while the PCT solution has a pH of 7. The presence of a negative charge on the surface of the photocatalyst, in conjunction with the anionic pollutant, will end up with a repulsive interaction between the nanocomposite photocatalyst and the pollutant. As a consequence, the adsorption of CPF and PCT on the surface of the CDs@ZnO-H400 catalyst nanocomposite is reduced, leading to a decline in the photocatalytic efficiency. The increase in photoactivity can be due to the improved adsorption of anionic pollutants on the surface of CDs@ZnO-H400 photocatalyst powder, which possesses a positive charge (Wannakan et al., 2023).

A research investigation was conducted to examine the impact of reactive species mechanisms on the photocatalytic degradation of

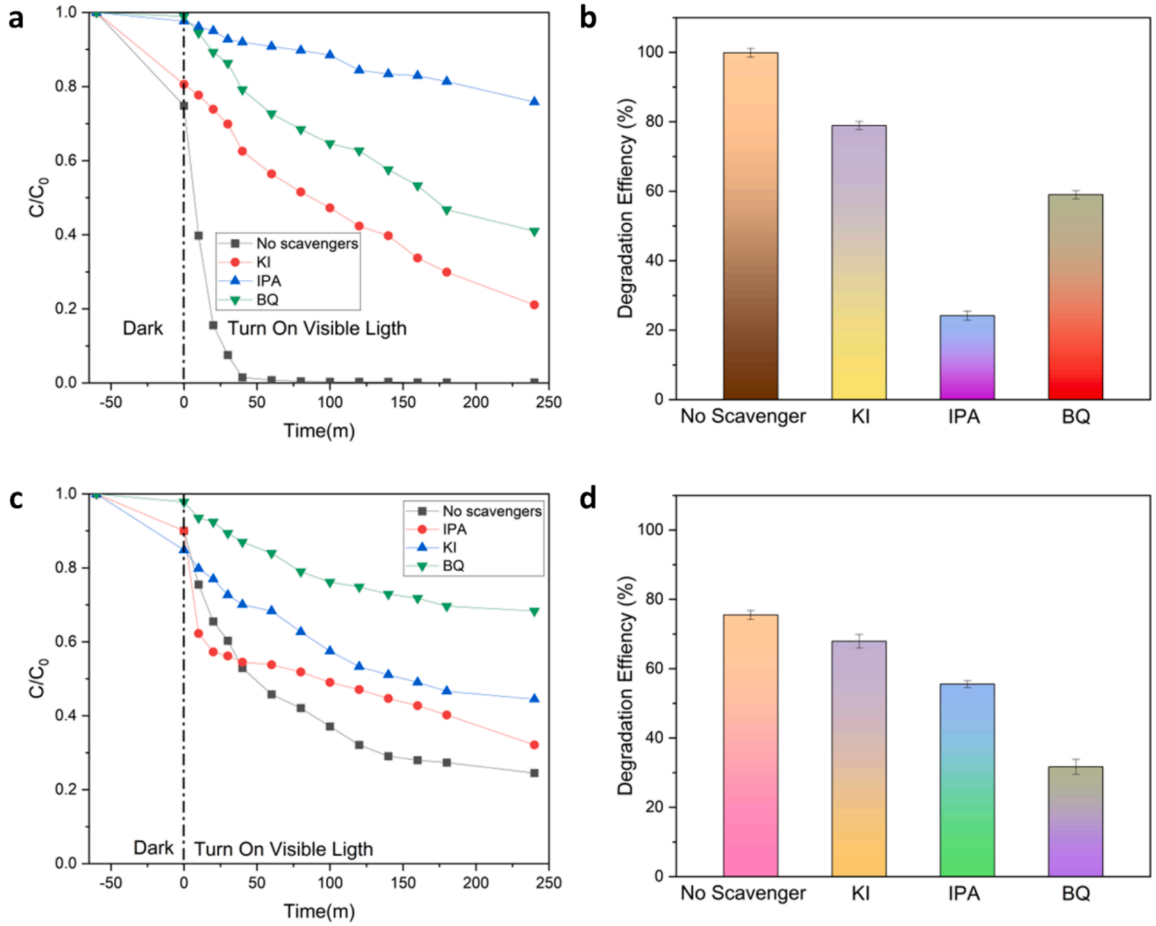

Fig. 6. Effect of various scavenger on degradation of Ciprofloxacin (a), the corresponding %degradation (b), of various scavenger on degradation of Paracetamol (c), and the corresponding %degradation (d). (n = 3).

CDs@ZnO-H400 in the degradation of CPF and PCT pollutants. Various scavengers, namely potassium iodide (KI), benzoquinone (BQ), and isopropyl alcohol (IPA), were introduced during the degradation process of each individual pollutant. The observed impact of KI, BQ, and IPA can be attributed to their different roles in regulating the activity of h^+, $^{\bullet}OH$, and $^{\bullet}O_2$. Fig. 6a and b demonstrate a decrease in the degradation of CPF with the addition of IPA, from 99 % to 27 %. This drop can be attributed to the significant role performed by $^{\bullet}OH$ in the degradation process of CPF. The impact of different scavengers on the degradation of PCT is illustrated in Fig. 6c and d. The addition of BQ resulted in a decrease in the degradation percentage from 75 % to 31 %. This decrease can be attributed to the significant role performed by $^{\bullet}O_2$ in the degradation process of PCT.

Photogeneration of the electrons and holes were occurred in the conduction band (C_B) and the valence band (V_B), respectively. After that, the formation of reactive species would be expected. In principle, the energy level of the C_B and V_B edges of both CDs@ZnO-H400 photocatalysts can be determined by using the Mulliken electronegativity theory as follows

$$E_{VB} = \chi - E_C + 0.5Eg \quad (9)$$

$$E_{CB} = E_{VB} - Eg \quad (10)$$

Where, E_{VB} represents the VB potential, E_{CB} denotes the CB potential, E_C stands for the standard hydrogen electrode potential (=4.5 eV), and represents the absolute value of the electronegativity of the semiconducting photocatalyst. The electronegativity values for ZnO were measured to be 5.79 eV. This resulted in charge separation and a good redox ability. The E_{VB} and E_{CB} values of CDs@ZnO-H400 were determined to be + 2.77 and −0.19 eV, respectively. Theoretically, the combined benefits of extended photo-absorption, exceptional charge separation, and a robust redox potential are achieved. The utilization of this heterojunction technique is highly suitable for implementation in the current study. Hence, Fig. 7 presents the propose mechanism for the photodegradation for elimination of pollutants using the CDs@ZnO-H400 heterojunction photocatalyst.

The practical application of the synthesized photocatalyst is significantly influenced by its reusability. Therefore, an investigation was conducted to examine the cycling capacity of the photocatalyst subsequent to the elimination of the CPF and PCT. The photocatalytic performance of the CDs@ZnO-H400 photocatalyst powder remains consistently high even after undergoing four cycles of utilization. After finished the first cycle, the powder has been filtered by using Whatman filter paper no1. After that it was dried in the oven for 24 h. This dry powder is ready to be used for another cycle. As seen in Fig. 8a, after 4 times cycling, the performance ability of catalyst powder CDs@ZnO-H400 was acceptable and stable in the process degradation of CPF and PCT. The crystal structure of the CDs@ZnO-H400 was also determined following the elimination of pollutants. The confirmation of the stability of the photocatalyst process will be conducted. Fig. 8b demonstrates that the XRD patterns of the photocatalyst before and after the photodegradation procedure were comparable, suggesting that the sample displayed excellent structural stability. The chemical bonding under FT-IR has been investigated for the fresh and used photocatalysts. As illustrated in Fig. 8c, The FT-IR spectra of the used and the fresh photocatalysts are similar, showing a high level of structural stability. Furthermore, an investigation was conducted on the morphological structure of the prepared CDs@ZnO-H400 using EDX-SEM, as depicted in Fig. 8d–i. The results demonstrate the stability of the morphology of CDs@ZnO-H400.

5. Conclusion

The CDs@ZnO-H400 heterojunction photocatalyst was produced via a hydrothermal technique, followed by calcination at a temperature of 400 °C. The CDs@ZnO-H400 heterostructure displayed a higher surface area compared to the monolayer CDs. The CDs@ZnO-H400 heterostructure photocatalyst exhibited a photocatalytic activity of 99.8 % and 75 % for the degradation of ciprofloxacin and paracetamol, respectively. The pollutant undergoes photodegradation following the first-order kinetic model. Even after enduring four cycles of usage, the photocatalyst consistently maintains remarkable performance, thereby indicating its promising ability to cycle. As a result, the system that was designed can help remove ciprofloxacin and paracetamol from the environment.

Author contributions

Material preparation, data collection were performed by David Nugroho, data analysis were performed by David Nugroho and Reggie Surya contributed to the study design and Supervision. Conceptualization was performed by, Aphinya Thinthasit, Khemika Wannakan, Suwat Nanan, and Rachadaporn Benchawattananon. The first draft of the manuscript was written by David Nugroho and Suwat Nanan was

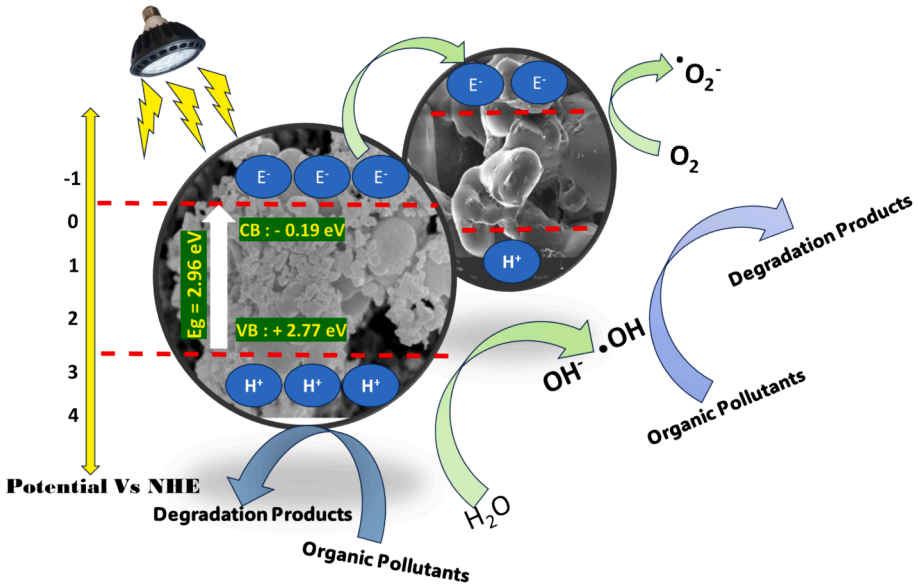

Fig. 7. Scheme prediction degradation of organic pollutants (Ciprofloxacin and Paracetamol).

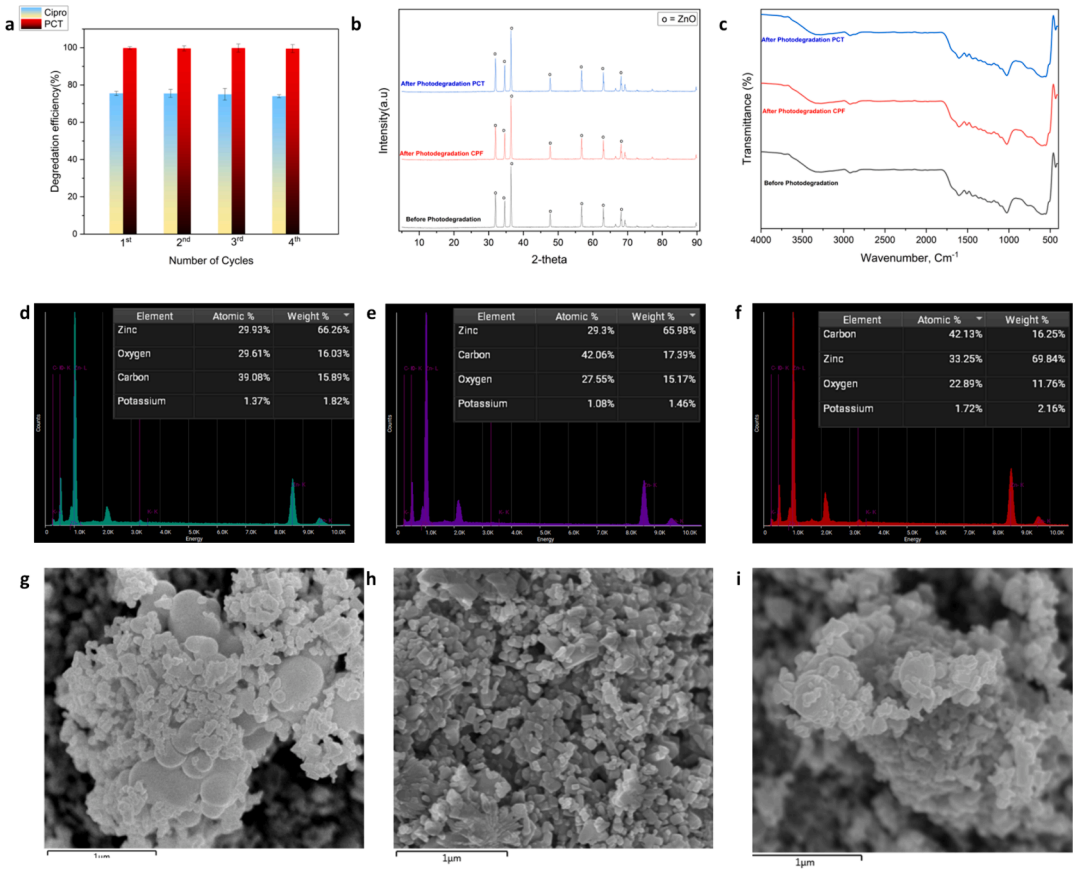

Fig. 8. (a) Reuse of photocatalyst for four cycles (a), XRD patterns (b), FTIR spectra (c) of the used and the fresh photocatalysts, EDX of the fresh catalyst (d) EDX of the used sample after degardation of ciprofloxacin (e), and paracetamol (f), micrographs of the fresh sample (g) and SEM of the used photocatalyst after degardation of ciprofloxacin (h), and paracetamol (i).

writing – review and editing the final draft of Manuscript. All authors read and approved the final manuscript.

CRediT authorship contribution statement

David Nugroho: Writing – original draft, Investigation, Data curation. **Aphinya Thinthasit:** Investigation, Data curation. **Khemika Wannakan:** Methodology, Investigation, Formal analysis, Data curation. **Reggie Surya:** Validation, Formal analysis, Data curation. **Suwat Nanan:** Writing – review & editing, Methodology, Investigation, Conceptualization. **Rachadaporn Benchawattananon:** Project administration, Conceptualization, Funding acquisition, Supervision.

Declaration of competing interest

The authors declare that they have no known competing financial interests or personal relationships that could have appeared to influence the work reported in this paper.

Acknowledgements

The authors would like to thank the Materials Chemistry Research Center (MCRC), Department of Chemistry, Faculty of Science, Center of Excellence for Innovation in Chemistry (PERCH-CIC), Khon Kaen University and Graduated School, Khon Kaen University.

References

Abdel-Wahab, A.M., Al-Shirbini, A.S., Mohamed, O., Nasr, O., 2017. Photocatalytic degradation of paracetamol over magnetic flower-like TiO_2/Fe_2O_3 core-shell nanostructures. J. Photochem. Photobiol. A Chem. 347, 186.

Aghamali, A., Khosravi, M., Hamishehkar, H., Modirshahla, N., Behnajady, M.A., 2018. Synthesis and characterization of high efficient photoluminescent sunlight driven photocatalyst of N-Carbon Quantum Dots. J. Lumin. 201, 265.

Agunbiade, F.O., Moodley, B., 2014. Pharmaceuticals as emerging organic contaminants in Umgeni River water system, KwaZulu-Natal, South Africa. *Environ. Monitor. Assess.* 186, 7273.

Ahlawat, A., Dhiman, T.K., Solanki, P.R., Rana, P.S., 2023. Facile synthesis of carbon dots via pyrolysis and their application in photocatalytic degradation of rhodamine B (RhB). Environ. Sci. Pollut. Res. 1.

Almeida, Â., Solé, M., Soares, A.M., Freitas, R., 2020. Anti-inflammatory drugs in the marine environment: Bioconcentration, metabolism and sub-lethal effects in marine bivalves. Environ. Pollut. 263, 114442.

Asadzadeh-Khaneghah, S., Habibi-Yangjeh, A., Nakata, K., 2019. Decoration of carbon dots over hydrogen peroxide treated graphitic carbon nitride: exceptional photocatalytic performance in removal of different contaminants under visible light. J. Photochem. Photobiol. A Chem. 374, 161.

Azuma, T., Otomo, K., Kunitou, M., Shimizu, M., Hosomaru, K., Mikata, S., Hayashi, T., 2019. Environmental fate of pharmaceutical compounds and antimicrobial-resistant bacteria in hospital effluents, and contributions to pollutant loads in the surface waters in Japan. Sci. Total Environ. 657, 476.

Bao, J., Shi, H., Huang, H., Ho, P.S., McSwiney, M.L., Goodner, M.D., Kloster, G.M., 2010. Oxygen plasma damage to blanket and patterned ultralow-κ surfaces. J. Vac. Sci. Technol. A 28 (2), 207.

Behera, A., Kandi, D., Mansingh, S., Martha, S., Parida, K., 2019. Facile synthesis of $ZnFe_2O_4$@ RGO nanocomposites towards photocatalytic ciprofloxacin degradation and H2 energy production. J. Colloid Interface Sci. 556, 667.

Benotti, M.J., Brownawell, B.J., 2007. Distributions of pharmaceuticals in an urban estuary during both dry-and wet-weather conditions. Environ. Sci. Tech. 41 (16), 5795.

Cai, J., Xin, W., Liu, G., Lin, D., Zhu, D., 2016. Effect of calcination temperature on structural properties and photocatalytic activity of Mn-C-codoped TiO_2. Mater. Res. 19, 401.

Chankhanittha, T., Watcharakitti, J., Nanan, S., 2019. PVP-assisted synthesis of rod-like ZnO photocatalyst for photodegradation of reactive red (RR141) and Congo red (CR) azo dyes. J. Mater. Sci. Mater. Electron. 30, 17804.
Chankhanittha, T., Komchoo, N., Senasu, T., Piriyanon, J., Youngme, S., Hemavibool, K., Nanan, S., 2021. Silver decorated ZnO photocatalyst for effective removal of reactive red azo dye and ofloxacin antibiotic under solar light irradiation. Colloids Surf A Physicochem Eng Asp 626, 127034.
Chehhat, K., Mecif, A., Mahdjoub, A.H., Nazir, R., Pandit, M.A., Salhi, F., Noua, A., 2023. Sol-gel synthesis of porous cobalt-doped ZnO thin films leading to rapid and large scale Orange-II photocatalysis. J. Sol-Gel Sci. Technol. 106 (1), 85.
Chen, T., Liu, S.Y., Xie, Q., Detavernier, C., Van Meirhaeghe, R.L., Qu, X.P., 2010. The effects of deposition temperature and ambient on the physical and electrical performance of DC-sputtered n-ZnO/p-Si heterojunction. Appl. Phys. A 98, 357.
Cheng, Y., Jin, J., Yan, H., Zhou, G., Xu, Y., Tang, L., Lu, Z., 2024. Spaced Double Hydrogen Bonding in an Imidazole Poly Ionic Liquid Composite for Highly Efficient and Selective Photocatalytic Air Reductive H_2O_2 Synthesis. Angew. Chem. 136 (15), e202400857.
Chopra, L., 2022. Photocatalytic activity of zinc oxide for dye and drug degradation: a review. Mater. Today:. Proc. 52, 1653.
Costa, T.M., Lima, M.S., Cruz Filho, J.F., Silva, L.J., Santos, R.S., Luz Jr, G.E., 2018. Synthesis, characterization, and photocatalytic activity of Ag_3PO_4/SBA-15 in ciprofloxacin degradation under polychromatic irradiation. J. Photochem. Photobiol. A Chem. 364, 461.
Dervishi, E., Ji, Z., Htoon, H., Sykora, M., Doorn, S.K., 2019. Raman spectroscopy of bottom-up synthesized graphene quantum dots: size and structure dependence. Nanoscale 11 (35), 16571.
Dou, B., Lan, J., Lang, S., Wang, Y., Yang, L., Liu, H., Lin, S., 2022. Multifunctional Ag/AgCl decorated CO_2-responsive cotton membranes with photo-induced self-cleaning property for efficient bidirectional oil/water separation and dyes removal. Polymer 251, 124890.
Ebert, I., Bachmann, J., Kühnen, U., Küster, A., Kussatz, C., Maletzki, D., Schlüter, C., 2011. Toxicity of the fluoroquinolone antibiotics enrofloxacin and ciprofloxacin to photoautotrophic aquatic organisms. Environ. Toxicol. Chem. 30 (12), 2786.
Fairbairn, D.J., Karpuzcu, M.E., Arnold, W.A., Barber, B.L., Kaufenberg, E.F., Koskinen, W.C., Swackhamer, D.L., 2016. Sources and transport of contaminants of emerging concern: A two-year study of occurrence and spatiotemporal variation in a mixed land use watershed. Sci. Total Environ. 551, 605.
Folawewo, A.D., Bala, M.D., 2022. Nanocomposite Zinc oxide-based photocatalysts: recent developments in their use for the treatment of dye-polluted wastewater. Water 14 (23), 3899.
Hou, X., Hu, Y., Wang, P., Yang, L., Al Awak, M.M., Tang, Y., Sun, Y.P., 2017. Modified facile synthesis for quantitatively fluorescent carbon dots. Carbon 122, 389.
Hu, X., Zhao, H., Liang, Y., Chen, F., Li, J., Chen, R., 2021. Broad-spectrum response NCQDs/$Bi_2O_2CO_3$ heterojunction nanosheets for ciprofloxacin photodegradation: Unraveling the unique roles of NCQDs upon different light irradiation. Chemosphere 264, 128434.
Huang, D., Zhou, H., Wu, Y., Wang, T., Sun, L., Gao, P., Hu, J., 2019. Bottom-up synthesis and structural design strategy for graphene quantum dots with tunable emission to the near infrared region. Carbon 142, 67.
Jallouli, N., Elghniji, K., Trabelsi, H., Ksibi, M., 2017. Photocatalytic degradation of paracetamol on TiO_2 nanoparticles and TiO2/cellulosic fiber under UV and sunlight irradiation. Arab. J. Chem. 10, S3640.
Kakarndee, S., Nanan, S., 2018. SDS capped and PVA capped ZnO nanostructures with high photocatalytic performance toward photodegradation of reactive red (RR141) azo dye. J. Environ. Chem. Eng. 6 (1), 7.
Khan, H.K., Rehman, M.Y.A., Malik, R.N., 2020. Fate and toxicity of pharmaceuticals in water environment: An insight on their occurrence in South Asia. J. Environ. Manage. 271, 111030.
Khan, S.H., Suriyaprabha, R., Pathak, B., Fulekar, M.H., 2015. Photocatalytic degradation of organophosphate pesticides (Chlorpyrifos) using synthesized zinc oxide nanoparticle by membrane filtration reactor under UV irradiation. Front. Nanosci. Nanotechnol. 1 (1), 23.
Li, N., Zhang, J., Tian, Y., Zhao, J., Zhang, J., Zuo, W., 2017. Precisely controlled fabrication of magnetic 3D γ-Fe_2O_3@ZnO core-shell photocatalyst with enhanced activity: ciprofloxacin degradation and mechanism insight. Chem. Eng. J. 308, 377.
Lin, Y.T., Weng, C.H., Lin, Y.H., Shiesh, C.C., Chen, F.Y., 2013. Effect of C content and calcination temperature on the photocatalytic activity of C-doped TiO_2 catalyst. Sep. Purif. Technol. 116, 114.
Liu, N., Lu, N., Su, Y., Wang, P., Quan, X., 2019. Fabrication of g-C_3N_4/Ti_3C_2 composite and its visible-light photocatalytic capability for ciprofloxacin degradation. Sep. Purif. Technol. 211, 782.
Lu, Z., Zhou, G., Song, M., Liu, X., Tang, H., Dong, H., Xing, G., 2020. Development of magnetic imprinted PEDOT/CdS heterojunction photocatalytic nanoreactors: 3-Dimensional specific recognition for selectively photocatalyzing danofloxacin mesylate. Appl. Catal. B 268, 118433.
Lu, Z., Zhou, G., Li, B., Xu, Y., Wang, P., Yan, H., Liu, X., 2022. Heterotopic reaction strategy for enhancing selective reduction and synergistic oxidation ability through trapping Cr (VI) into specific reaction site: A stable and self-cleaning ion imprinted CdS/HTNW photocatalytic membrane. Appl. Catal. B 301, 120787.
Manu, B., Mahamood, S., Vittal, H., Shrihari, S., 2011. A novel catalytic route to degrade paracetamol by Fenton process. IJRCE 1, 157.
Meky, A.I., Hassaan, M.A., Fetouh, H.A., Ismail, A.M., El Nemr, A., 2024. Hydrothermal fabrication, characterization and RSM optimization of cobalt-doped zinc oxide nanoparticles for antibiotic photodegradation under visible light. Sci. Rep. 14 (1), 2016.
Mukherjee, I., Cilamkoti, V., Dutta, R.K., 2021. Sunlight-driven photocatalytic degradation of ciprofloxacin by carbon dots embedded in ZnO nanostructures. ACS Appl. Nano Mater. 4 (8), 7686.
Nie, J., Yu, X., Liu, Z., Wei, Y., Zhang, J., Zhao, N., Yao, B., 2022. Boosting principles for the photocatalytic performance of Cr-dopedCu_2O crystallites and mechanisms of photocatalytic oxidation for levofloxacin. Appl. Surf. Sci. 576, 151842.
Nugroho, D., Keawprom, C., Chanthai, S., Oh, W.C., Benchawattananon, R., 2022. Highly sensitive fingerprint detection under UV light on non-porous surface using starch-powder based luminol-doped carbon dots (N-CDs) from tender coconut water as a green carbon source. Nanomaterials 12 (3), 400.
Nugroho, D., Oh, W.C., Chanthai, S., Benchawattananon, R., 2022. Improving minutiae image of latent fingerprint detection on non-porous surface materials under UV light using sulfur doped carbon quantum dots from Magnolia grandiflora flower. Nanomaterials 12 (19), 3277.
Nugroho, D., Wannakan, K., Nanan, S., Benchawattananon, R., 2024. The Synthesis of carbon dots//zincoxide (CDs/ZnO-H400) by using hydrothermal methods for degradation of ofloxacin antibiotics and reactive red azo dye (RR141). Sci. Rep. 14 (1), 2455.
Nugroho, D., Thinthasit, A., Khoris, I.M., Siriputthaiwan, P., Benchawattananon, R., Chanthai, S., 2024. L-histidine doped CDs from Zingiber Montanum using hydrothermal method to enhance its antimicrobial activity and imply for latent fingerprint detection. Arab. J. Chem. 17 (3), 105602.
Patel, M., Kumar, R., Kishor, K., Mlsna, T., Pittman Jr, C.U., Mohan, D., 2019. Pharmaceuticals of emerging concern in aquatic systems: chemistry, occurrence, effects, and removal methods. Chem. Rev. 119 (6), 3510.
Queiróz, A.C.B., Santos, A.P., Queiroz, T.S., Lima, A.E., da Silva, R.M.P., Antunes, R.A., Caldeira, V.P., 2023. Ciprofloxacin photodegradation by CeO_2 nanostructures with different morphologies. Water Air Soil Pollut. 234 (7), 415.
Raja, J., Nguyen, C.P.T., Lee, C., Balaji, N., Chatterjee, S., Jang, K., Yi, J., 2016. Improved data retention of InSnZnO nonvolatile memory by H_2O_2 treated Al_2O_3 tunneling layer: A cost-effective method. IEEE Electron Device Lett. 37 (10), 1272.
Rajia, S., Hasan, I., Amin, R., Islam, M.A.U., 2015. Efficiency of a cost-effective UV spectrophotometric method for estimation of ciprofloxacin HCl in marketed tablet formulation. Int. J. Pharm. Sci. Res. 6 (10), 4277.
Ramos, P.G., Espinoza, J., Sánchez, L.A., Rodriguez, J., 2023. Enhanced photocatalytic degradation of Rhodamine B employing transition metal (Fe, Cu, Co) doped ZnO/rGO nanostructures synthesized by electrospinning-hydrothermal technique. J. Alloy. Compd. 966, 171559.
Sanchez Tobon, C., Ljubas, D., Mandić, V., Panžić, I., Matijašić, G., Ćurković, L., 2022. Microwave-assisted synthesis of N/TiO2 nanoparticles for photocatalysis under different irradiation spectra. Nanomaterials 12 (9), 1473.
Senasu, T., Chankhanittha, T., Hemavibool, K., Nanan, S., 2021. Visible-light-responsive photocatalyst based on ZnO/CdS nanocomposite for photodegradation of reactive red azo dye and ofloxacin antibiotic. Mater. Sci. Semicond. Process. 123, 105558.
Senasu, T., Chankhanittha, T., Hemavibool, K., Nanan, S., 2022. Solvothermal synthesis of BiOBr photocatalyst with an assistant of PVP for visible-light-driven photocatalytic degradation of fluoroquinolone antibiotics. Catal. Today 384, 209.
Senasu, T., Ruengchai, N., Khamdon, S., Lorwanishpaisarn, N., Nanan, S., 2022. Hydrothermal synthesis of cadmium sulfide photocatalyst for detoxification of azo dyes and ofloxacin antibiotic in wastewater. Molecules 27 (22), 7944.
Song, M., de Villiers, M.M., 2005. Effect of a change in crystal polymorph on the degree of adhesion between micronized drug particles and large homogenous carrier particles during an interactive mixing process. Pharm. Dev. Technol. 9 (4), 387.
Swapna, M.S., Sankararaman, S., 2019. Thermal induced order fluctuations in carbon nanosystem with carbon nanotubes. Nano-Struct. Nano-Objects 19, 100375.
Thi, V.H.T., Lee, B.K., 2017. Effective photocatalytic degradation of paracetamol using La-doped ZnO photocatalyst under visible light irradiation. Mater. Res. Bull. 96, 171.
Togola, A., Budzinski, H., 2008. Multi-residue analysis of pharmaceutical compounds in aqueous samples. J. Chromatogr. A 1177 (1), 150.
Trujillano, R., Rives, V., García, I., 2022. Photocatalytic degradation of paracetamol in aqueous medium using TiO_2 prepared by the sol–gel method. Molecules 27 (9), 2904.
Van Thuan, D., Nguyen, T.B., Pham, T.H., Kim, J., Chu, T.T.H., Nguyen, M.V., Elshikh, M. S., 2022. Photodegradation of ciprofloxacin antibiotic in water by using ZnO-doped g-C3N4 photocatalyst. Chemosphere 308, 136408.
Wang, Y., Wang, F., Feng, Y., Xie, Z., Zhang, Q., Jin, X., Liu, G., 2018. Facile synthesis of carbon quantum dots loaded with mesoporous gC 3 N 4 for synergistic absorption and visible light photodegradation of fluoroquinolone antibiotics. Dalton Trans. 47 (4), 1284.
Wang, Y., Yang, L., Zou, R., Lan, J., Yao, A., Xiao, H., Lin, S., 2022. Z-scheme CeO_2/Ag/CdS heterojunctions functionalized cotton fibers as highly recyclable and efficient visible light-driven photocatalysts for the degradation of dyes. J. Clean. Prod. 380, 135012.
Wannakan, K., Khansamrit, K., Senasu, T., Nanan, S., 2023. Ultrasound-assisted synthesis of a ZnO/$BiVO_4$ S-scheme heterojunction photocatalyst for degradation of the reactive red 141 dye and oxytetracycline antibiotic. ACS Omega 8 (5), 4835.
Xu, D., Fan, D., Shen, W., 2013. Catalyst-free direct vapor-phase growth of Zn 1–x Cu x O micro-cross structures and their optical properties. Nanoscale Res. Lett. 8, 1.
Xu, J.J., Lu, Y.N., Tao, F.F., Liang, P.F., Zhang, P.A., 2023. ZnO nanoparticles modified by carbon quantum dots for the photocatalytic removal of synthetic pigment pollutants. ACS Omega 8 (8), 7845.
Xu, Y., Zhu, X., Yan, H., Wang, P., Song, M., Ma, C., Lu, Z., 2022. Hydrochloric acid-mediated synthesis of ZnFe2O4 small particle decorated one-dimensional Perylene Diimide S-scheme heterojunction with excellent photocatalytic ability. Chin. J. Catal. 43 (4), 1111.

Xu, Y., Ren, Y., Zhou, G., Feng, S., Yang, Z., Dai, S., Zhou, T., 2024. Amide-engineered metal-organic porous liquids toward enhanced CO_2 photoreduction performance. Adv. Funct. Mater., 2313695

Yan, X., Xu, T., Chen, G., Yang, S., Liu, H., Xue, Q., 2004. Preparation and characterization of electrochemically deposited carbon nitride films on silicon substrate. J. Phys. D Appl. Phys. 37 (6), 907.

Yan, Y., Zhai, D., Liu, Y., Gong, J., Chen, J., Zan, P., Chen, P., 2020. van der Waals heterojunction between a bottom-up grown doped graphene quantum dot and graphene for photoelectrochemical water splitting. ACS Nano 14 (1), 1185.

Yang, L., Liya, E.Y., Ray, M.B., 2008. Degradation of paracetamol in aqueous solutions by TiO_2 photocatalysis. Water Res. 42 (13), 3480.

Yang, S., Xu, D., Chen, B., Luo, B., Shi, W., 2017. In-situ synthesis of a plasmonic Ag/AgCl/Ag_2O heterostructures for degradation of ciprofloxacin. Appl. Catal. B 204, 602.

Yang, F., Yu, X., Wang, K., Liu, Z., Gao, Z., Zhang, T., Yao, B., 2023. Photocatalytic degradation of methylene blue over $BiVO_4$/$BiPO_4$/rGO heterojunctions and their artificial neural network model. J. Alloy. Compd. 960, 170716.

Yu, X., Chen, H., Ji, Q., Chen, Y., Wei, Y., Zhao, N., Yao, B., 2021. p-Cu_2O/n-ZnO heterojunction thin films with enhanced photoelectrochemical properties and photocatalytic activities for norfloxacin. Chemosphere 267, 129285.

Yu, J., Sun, H., Zheng, C., Wang, J., Wang, H., Tao, H., Zhang, Z., 2024. Improved photocatalytic performance of Sn/Cl co-doped TiO_2 nanoparticles via a novel volatilization solid solution method. Opt. Mater. 151, 115417.

Yu, X., Zhang, J., Chen, Y., Ji, Q., Wei, Y., Niu, J., Yao, B., 2021. Ag-Cu_2O composite films with enhanced photocatalytic activities for methylene blue degradation: analysis of the mechanism and the degradation pathways. J. Environ. Chem. Eng. 9 (5), 106161.

Zhang, G., Cheng, R., Yan, J., Xiao, Y., Zang, C., Zhang, Y., 2021. Photodegradation property and antimicrobial activity of zinc oxide nanorod-coated polypropylene nonwoven fabric. Polym. Test. 100, 107235.

Zhao, J., Nan, J., Zhao, Z., Li, N., 2017. Facile fabrication of novel Mn_2O_3 nanocubes with superior light-harvesting for ciprofloxacin degradation. Catal. Commun. 102, 5.

Zhou, G., Xu, Y., Cheng, Y., Yu, Z., Wei, B., Liu, X., Lu, Z., 2023. Rapid dissociation of high concentration excitons between $[Bi_2O_2]^{2+}$ slabs with multifunctional N-Bi-O sites for selective photoconversion into CO. Appl. Catal. B 335, 122892.

Zou, R., Li, L., Yang, L., Lan, J., Liu, H., Dou, B., Lin, S., 2021. CeO_2/CdS heterojunction decorated cotton fabric as a recyclable photocatalyst for efficient light driven degradation of methylene blue. Cellul. 28, 11081.